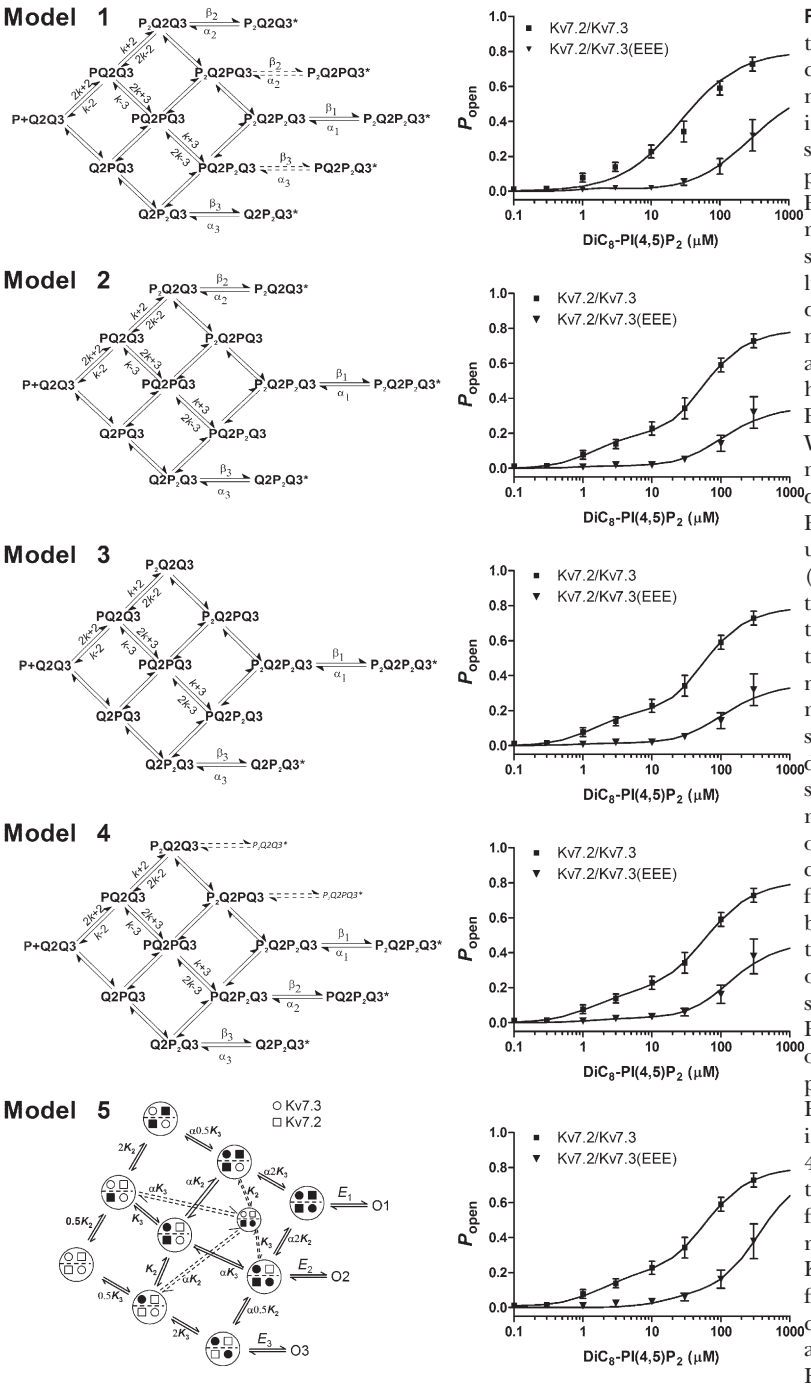

Figure S1. Development of a subunit-specific model to describe M-channel activation by PI(4,5)P_2. M channels are likely to be assembled from two heterodimers composed of a Kv7.2 and a Kv7.3 subunit, creating a channel, composed of a pair of dimers of subunits arranged symmetrically around a central pore. This arrangement is assumed to create two PI(4,5)P_2 binding sites of equal (low) affinity (equilibrium constant K_2) and two equal PI(4,5)P_2 binding sites of high affinity (equilibrium constant K_3), as illustrated schematically in Fig. 6 A. Assuming independent binding of PI(4,5)P_2 to each subunit requires a model with four separate PI(4,5)P_2 binding reactions, as illustrated in Fig. 6 A (S1–S4). To gain insight into how channel opening is related to binding of PI(4,5)P_2, each of these models was fitted to the data sets for WT Kv7.2/Kv7.3 channels and for Kv7.2/Kv7.3(EEE) mutant channels. Parameter values for the fits to each data set are given in Table S1. In each model, PI(4,5)P_2 is represented by P, whereas Kv7.2 and Kv7.3 subunits are represented as Q2 and Q3, respectively. (model 1) This model assumes that at least three of the four PI(4,5)P_2 binding sites need to be occupied to trigger channel opening. The parameter values for this model illustrate that the value for K_3 is not determined. This model cannot produce the two-component activation curve observed experimentally and, so, was rejected. (model 2) In contrast, this model does produce a two-component activation curve and, so, is a candidate mechanism to describe the M channel. The fit of this mechanism to the data predicts that openings where only the two low-affinity states are occupied will be extremely rare (peak open probability for the P_2Q2Q3* state of $<10^{-6}$). In addition, it might be expected that if channels can open when only the two high-affinity sites are occupied, they may also open when these two sites and one of the low-affinity sites are occupied. (model 3) This model lacks the P_2Q2Q3* (open state in which both Kv7.2 subunits are occupied by PIP_2 but the Kv7.3 subunits are unoccupied) and can provide a reasonable fit to the data. However, as with model 2, it seems unlikely that openings from the $PQ2P_2Q3$ state would not occur. (model 4) Including opening of the $PQ2P_2Q3$ state improves the model fit (reduced sum of squares) and was therefore selected as the model most consistent with current structural and functional knowledge of Kv7.2/Kv7.3 and related channels. In principle, openings from channels in which the two Kv7.2 subunits are occupied by PI(4,5)P_2 (P_2Q2Q3 and P_2Q2PQ3) might also occur. These are indicated by the dashed lines. However, because of the low binding affinity of PI(4,5)P_2 to the Kv7.2 subunits, in practice, such openings are very rare and do not make a detectable contribution to the overall open probability of the heteromer and, so, have been ignored. The presence of three open states might also be resolved with the previous kinetic analyses identifying only two open states if the small contribution of the triliganded $PQ2P_2Q3$ to the overall channel activity was not readily detected as a separate kinetic state (e.g., if the lifetime of open state O2 was similar to that of O3). (model 5) The possibility of cooperativity between PIP_2 binding sites was explored using a subunit dimer–dependent cooperativity model. In this case, the M channel is assumed to function as a dimer of dimers, and binding at one subunit within the dimer can then influence the affinity of the adjacent subunit but not the affinities of the subunits in the alternate dimer (for clarity, dimers are shown separated by dashed lines). Occupancy of each binding site, Kv7.2 (squares) and Kv7.3 (circles), is indicated by filled symbols. The presence of cooperativity within dimers creates an extra kinetic state, indicated as connected by dashed lines in the diagram. Cooperativity is quantified by the constant α, the factor by which the equilibrium constant for a binding site is multiplied when the adjacent binding site is occupied. It is negative cooperativity if α > 1. Data points show mean ± SEM; Kv7.2/Kv7.3, n = 20–49 patches; Kv7.2/Kv7.3(EEE), n = 8–13 patches.

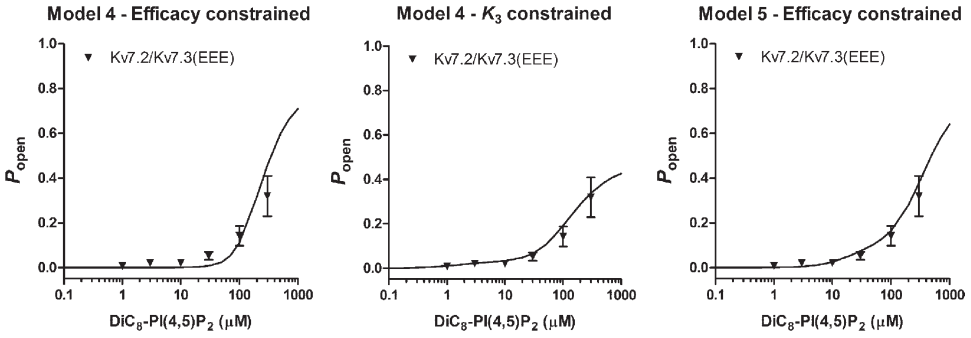

Figure S2. Investigation of the contribution of changes in binding affinity and gating efficiency to the overall effect of the Kv7.3(EEE) mutation. To gain insight into the effect of the Kv7.3(EEE) mutation, model 4 was used to investigate whether the effect of this mutation could be explained entirely on the basis of a decrease in the binding affinity of DiC_8-PI(4,5)P_2 with no change compared with WT receptors in gating efficiency (left). Alternatively, if the change in binding affinity caused by this mutation was constrained to be as predicted from the change in free energy (ΔG) estimated from phosphoinositide-docking simulations for WT and Kv7.3(EEE) mutant channels (Hernandez et al., 2009), then how much would the gating efficiency of the Kv7.2/Kv7.3(EEE) need to have changed compared with the WT channels to adequately describe the data? In each case, the affinity of the Kv7.2 binding site was constrained to have the same affinity as estimated from fitting the WT data (K_2 = 96 μM). Constraining the gating efficiency constants E_1, E_2, and E_3 to be the same as the WT data gives an estimate for the affinity of the Kv7.3(EEE) mutant channels of K_3 = 241 μM and a predicted P_{open} curve that does not follow well with the data points (left), resulting in an approximately 10-fold increase in the sum of squares (=0.3928) for the fit. In contrast, constraining the value of K_3 according to that predicted from the free energy calculations of Hernandez et al. (2009) (Kv7.3 binding ΔG = −14.1 $kJmol^{-1}$ and Kv7.3(EEE) binding ΔG = −6.3 $kJmol^{-1}$) indicated a 24.6-fold change in affinity. Our estimate for WT Kv7.3 affinity (K_3 = 0.94 μM) therefore translates into a predicted microscopic affinity for the Kv7.3(EEE) mutant of K_3 = 23.2 μM. Constraining the model fitting with this value for K_3 results in a reasonable approximation to the data points (middle), provided the values for E_1, E_2, and E_3 are allowed to decrease substantially relative to WT channels (Table S1). Thus, the conclusion from fitting model 4 to these data is that the Kv7.3(EEE) mutation is a mutation that substantially affects the efficiency of coupling of PI(4,5)P_2 binding to channel gating. An alternative hypothesis regarding the effect of the Kv7.3(EEE) mutation is that it may affect cooperativity in binding between PIP_2 binding sites. To test this idea, we fit model 5 to WT and Kv7.3(EEE) mutant channel data and then tested whether this model could fit the Kv7.3(EEE) mutant data if the gating efficiency constants E_1, E_2, and E_3 were constrained to have the same values as the WT channel. With this constraint, a reasonable fit to the Kv7.3(EEE) mutant data is achieved (right; Table S3), with the predicted value for K_3 of 23.1 μM being very similar to that calculated from the free energy calculations of Hernandez et al. (2009). However, the sum of squares is 166 times bigger when the efficacy of the mutant channel is constrained to be the same as the WT. Thus, the improved fit achieved by including an approximately fivefold increase in negative cooperativity for the Kv7.3(EEE) mutant does not compensate for the change in apparent efficacy suggested by the model fits to the Kv7.3(EEE) mutant (data points show mean ± SEM; Kv7.2/Kv7.3(EEE), n = 8–13 patches).

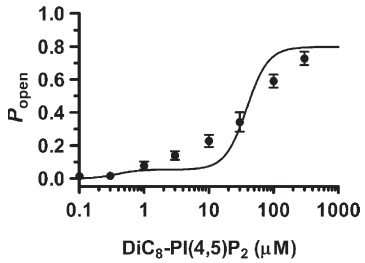

Figure S3. Fidelity of channel subunit assembly. Fitting the M-channel data to a kinetic model requires the assumption that the channels are a homogeneous population. Here, we assess one possible cause of heterogeneity: variation in subunit stoichiometry when expressing Kv7.2 and Kv7.3 subunits together. Assuming that channel subunits can assemble randomly, the number (N) of possible subunit combinations was calculated from

$$N = \frac{n!}{p! \times q!},$$

where n is the number of subunits forming the channel ($n = 4$), p is number of Kv7.2, and q is number of Kv7.3 subunits. The proportions of each channel type (Kv7.2 homomer, Kv7.3 homomer, etc.) are listed in Table S4. The rotational symmetry of a tetramer means that most variations in the order of subunits around the pore produce equivalent channels. With these considerations, five different types of M channel may arise from random assembly of Kv7.2 and Kv7.3 subunits. As in previous simulations of M-channel activity (e.g., Hernandez et al. [2009]), we assume here that all subunits need to have PIP_2 bound before the channel opens. In addition, we assumed each subunit contributes equally to gating the channel and that the maximum P_{open} for each type of channel = 0.8. The mean P_{open} for this population of channels was then fit by weighted least squares to the Kv7.2/Kv7.3 data, with the proportions of the channels fixed as dictated by random subunit assembly while allowing the values for PIP_2 affinity at the Kv7.2 and Kv7.3 subunits to vary. The best-fit values for K_2 and K_3 were 38 and 0.36 μM. However, the most obvious feature of this model is that the P_{open} curve is much steeper for the model than for the data (data points show mean ± SEM; Kv7.2/Kv7.3, n = 20–49 patches).

TABLE S1

Model-fitted parameters

	Model 1		Model 2		Model 3		Model 4		Model 5	
	WT	Q3(EEE)	WT	Q3(EEE)	WT	Q3(EEE)	WT	Q3(EEE)	WT	Q3(EEE)
K_2 (μM)	134.5	134.5	65.90	65.9	65.81	65.81	96.09	96.09	55.63	55.63
K_3 (μM)	0.01	0.722	1.11	0.51	1.11	0.51	0.84	0.94	1.43	0.99
E_1	4.07	1.573	3.96	0.56	3.96	0.56	4.42	0.89	3.99	2.23
E_2	1.56	324	0.00	0.001	ND	ND	0.46	0.00	0.18	0.11
E_3	2.03	0.093	0.36	0.02	0.36	0.02	0.26	0.04	0.36	0.04
α									1.38	5.36
P_o (max)	0.803	0.611	0.80	0.359	0.80	0.358	0.82	0.47	0.80	0.69
SSQ	0.4395	0.05	0.0408	0.0478	0.0410	0.0479	0.0334	0.0353	0.0145	0.00039

SSQ, sum of squares.

TABLE S2

Parameter estimates from fitting Kv7.3(EEE) mutant channels to model 4 with efficacy or affinity constraints

Kv7.2/Kv7.3(EEE)	Free fit	E_1, E_2, and E_3 constrained	K_3 constrained
K_2 (μM)	96.0	96.0	96.0
K_3 (μM)	0.94	241.0	23.2
E_1	0.89	4.42	1.07
E_2	0.00	0.46	0.00
E_3	0.04	0.26	0.28
P_o (max)	0.47	0.816	0.516
SSQ	0.0353	0.3928	0.0899

See Fig. S2 text for further details. SSQ, sum of squares.

TABLE S3

Parameter estimates from fitting Kv7.3(EEE) mutant channels to a subunit dimer–dependent cooperativity model (model 5)

	Kv7.2/Kv7.3	Kv7.2/Kv7.3(EEE)	Kv7.2/Kv7.3(EEE) efficacy constrained
K_2 (μM)	55.63	55.63	55.63
K_3 (μM)	1.43	0.99	23.1
E_1	3.99	2.23	3.99
E_2	0.18	0.11	0.18
E_3	0.36	0.04	0.36
α	1.38	5.36	6.645
SSQ	0.0145	0.00039	0.06518

See Figs. S1 (model 5) and S2 (right graph) with efficacy constraints. SSQ, sum of squares.

TABLE S4

Proportions of channel subtypes created with a random subunit assembly model and parameter estimates obtained by fitting the data with this model

Subunit composition	Proportions
2-2-2-2	0.0625
2-2-2-3	0.25
2-2-3-3 and 2-3-2-3	0.375
2-3-3-3	0.25
3-3-3-3	0.0625
K_2 (μM)	38.2
K_3 (μM)	0.36